

Supplementary Information for:

**Thermoelectric properties of the aliovalent half-Heusler alloy  $\text{Zn}_{0.5}\text{Ti}_{0.5}\text{NiSb}$  with intrinsic low thermal conductivity**

Blair F. Kennedy<sup>1</sup>, Simon A. J. Kimber,<sup>2</sup> Stefano Checchia,<sup>3</sup> A. K. M. Ashiquzzaman Shawon,<sup>5</sup>  
Alexandra Zevalkink,<sup>5</sup> Emmanuelle Suard<sup>6</sup>, Jim Buckman<sup>7</sup> and Jan-Willem G. Bos<sup>4</sup>

*1. Institute of Chemical Sciences, School of Engineering and Physical Sciences, Heriot-Watt University, Edinburgh, EH14 4AS, UK.*

*2. Université Bourgogne Franche-Comté, Université de Bourgogne, Nanosciences Department, ICB-Laboratoire Interdisciplinaire Carnot de Bourgogne, Bâtiment Sciences Mirande, Dijon, France.*

*3. ESRF, The European Synchrotron, 71 Avenue des Martyrs, CS40220, 38043 Grenoble Cedex 9, France.*

*4. EaStCHEM School of Chemistry, University of St Andrews, North Haugh, St Andrews, KY16 9ST, UK.*

*5. Chemical Engineering and Materials Science Department, Michigan State University, East Lansing, Michigan 48824, USA.*

*6. Institut Laue-Langevin (ILL), BP 156, 71 Avenue des Martyrs, 38042 Grenoble, France*

*7. School of Energy, Geoscience, Infrastructure and Society, Heriot-Watt University, Edinburgh, EH14 4AS, UK.*

**Email:** [j.w.g.bos@st-andrews.ac.uk](mailto:j.w.g.bos@st-andrews.ac.uk)

**Table S1:** Half-Heusler compositions for hot-pressed  $\text{Zn}_{1-x}\text{Ti}_x\text{NiSb}$  disks derived from EDX elemental maps shown in Fig. S1.

<b>Nominal Composition</b>	<b>EDX Composition</b>
$\text{Zn}_{0.35}\text{Ti}_{0.65}\text{NiSb}$	$\text{Zn}_{0.32}\text{Ti}_{0.65}\text{NiSb}_{1.02}$
$\text{Zn}_{0.40}\text{Ti}_{0.60}\text{NiSb}$	$\text{Zn}_{0.39}\text{Ti}_{0.61}\text{NiSb}$
$\text{Zn}_{0.45}\text{Ti}_{0.55}\text{NiSb}$	$\text{Zn}_{0.42}\text{Ti}_{0.54}\text{NiSb}_{1.03}$
$\text{Zn}_{0.50}\text{Ti}_{0.50}\text{NiSb}$	$\text{Zn}_{0.47}\text{Ti}_{0.53}\text{NiSb}$
$\text{Zn}_{0.55}\text{Ti}_{0.45}\text{NiSb}$	$\text{Zn}_{0.55}\text{Ti}_{0.46}\text{NiSb}_{1.02}$
$\text{Zn}_{0.60}\text{Ti}_{0.40}\text{NiSb}$	$\text{Zn}_{0.58}\text{Ti}_{0.41}\text{NiSb}_{1.01}$

**Table S2:** Overview of resistivity fit parameters for the  $\text{Zn}_{1-x}\text{Ti}_x\text{NiSb}$  samples,<sup>1</sup> see manuscript for further details.

	$E_g$ (eV)	$\rho_0$ ( $\mu\Omega\cdot\text{m}$ )	$B(\times 10^{-4} \mu\Omega\cdot\text{m}\cdot\text{K}^{-1.5})$	$A$ ( $\mu\Omega\cdot\text{m}$ )	$\rho_0/B$ ( $\text{K}^{1.5}$ )
<b>n-type</b>					
$\text{Zn}_{0.35}\text{Ti}_{0.65}\text{NiSb}$	0.39 (fixed)	7(1)	2.5(3)	5.4(1)	27500
$\text{Zn}_{0.40}\text{Ti}_{0.60}\text{NiSb}$	0.39 (fixed)	14(1)	4.7(3)	4.0(1)	29978
$\text{Zn}_{0.45}\text{Ti}_{0.55}\text{NiSb}$	0.39(2)	33(3)	-	2.0(1)	-
<b>p-type</b>					
$\text{Zn}_{0.50}\text{Ti}_{0.50}\text{NiSb}$	0.39(2)	53(3)	-	2.1(1)	-
$\text{Zn}_{0.55}\text{Ti}_{0.45}\text{NiSb}$	0.39 (fixed)	15(1)	-	1.8(1)	-
$\text{Zn}_{0.60}\text{Ti}_{0.40}\text{NiSb}$	0.39 (fixed)	7(1)	0.7(1)	1.9(1)	105980

**Table S3:** Measured, crystallographic and % density of the hot pressed  $\text{Zn}_{1-x}\text{Ti}_x\text{NiSb}$  ( $0.4 \leq x \leq 0.65$ ) disks characterised in this manuscript.

<b>Composition</b>	<b>Measured Density (<math>\text{g}\cdot\text{cm}^{-3}</math>)</b>	<b>Crystallographic Density (<math>\text{g}\cdot\text{cm}^{-3}</math>)</b>	<b>% Density</b>
$\text{Zn}_{0.35}\text{Ti}_{0.65}\text{NiSb}$	7.37(2)	7.58	97.2
$\text{Zn}_{0.40}\text{Ti}_{0.60}\text{NiSb}$	7.41(2)	7.58	97.7
$\text{Zn}_{0.45}\text{Ti}_{0.55}\text{NiSb}$	7.48(2)	7.59	98.5
$\text{Zn}_{0.50}\text{Ti}_{0.50}\text{NiSb}$	7.5(2)	7.60	98.7
$\text{Zn}_{0.55}\text{Ti}_{0.45}\text{NiSb}$	7.51(2)	7.60	98.8
$\text{Zn}_{0.60}\text{Ti}_{0.40}\text{NiSb}$	7.56(2)	7.61	99.3

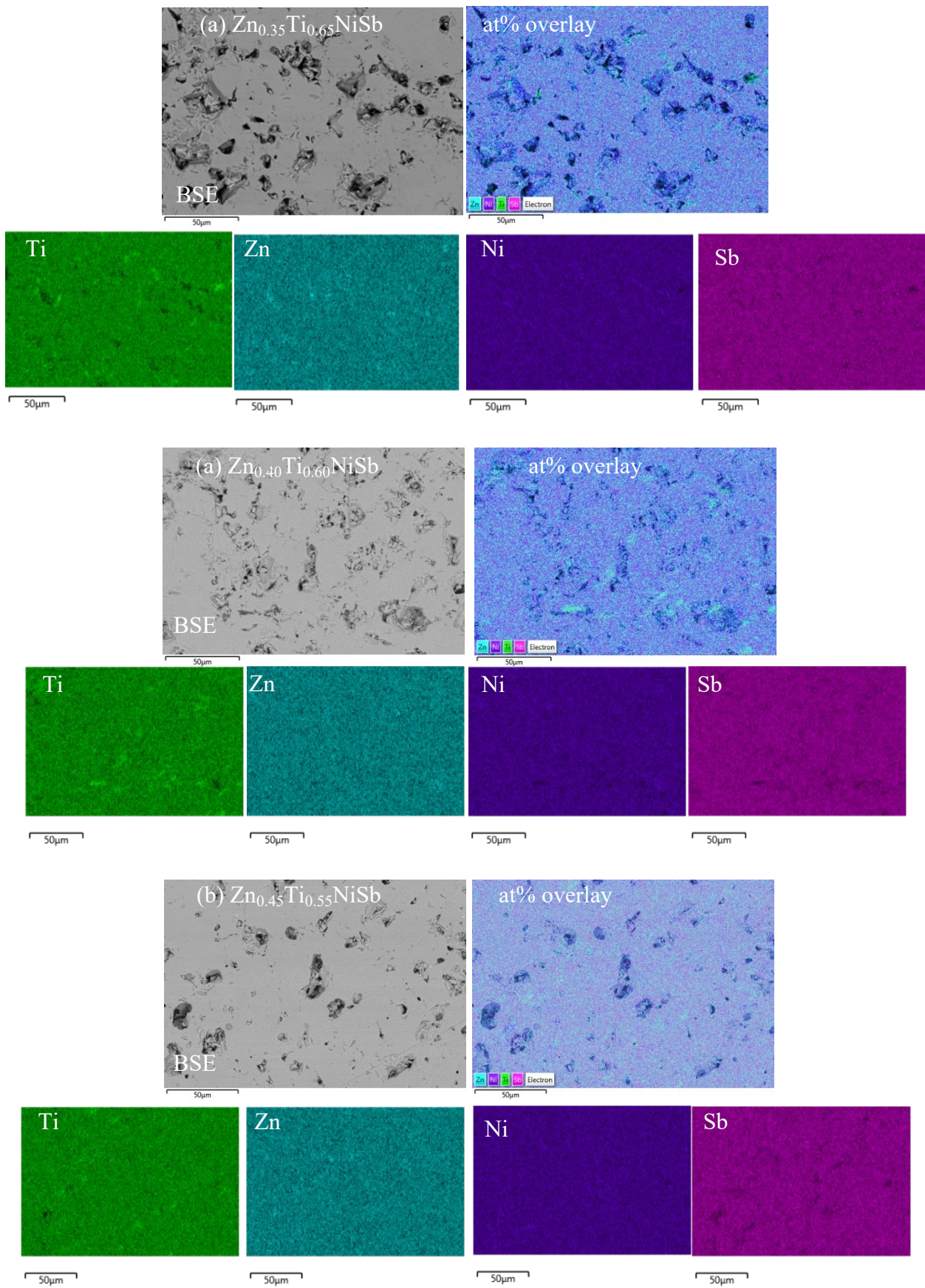


**Figure S1:** Backscattered Secondary Electron SEM images, at% composite and individual elemental at% maps for n-type Zn<sub>1-x</sub>Ti<sub>x</sub>NiSb disks.

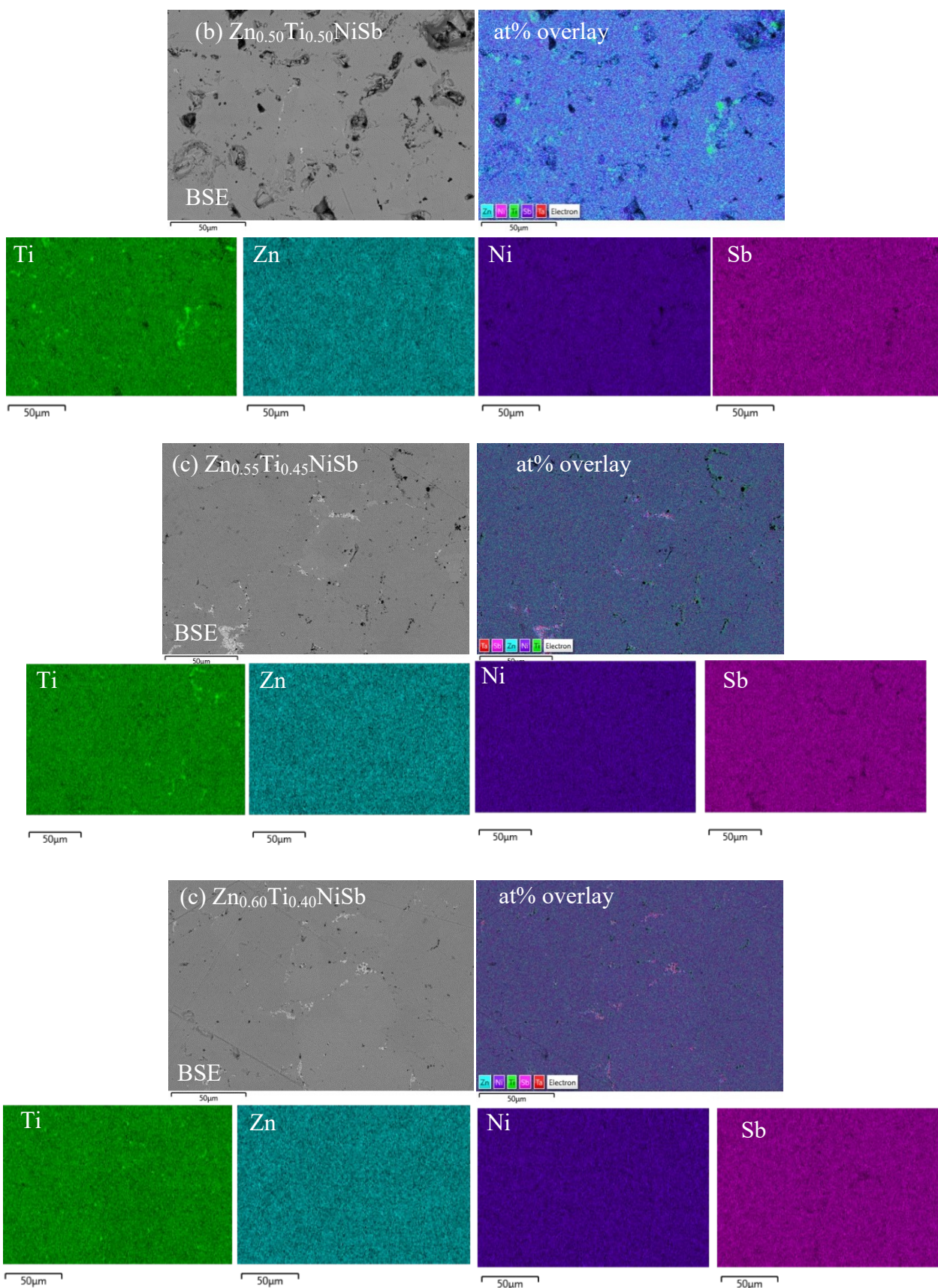


**Figure S2:** Backscattered Secondary Electron SEM images, at% composite and individual elemental at% maps for p-type  $Zn_{1-x}Ti_xNiSb$  disks.

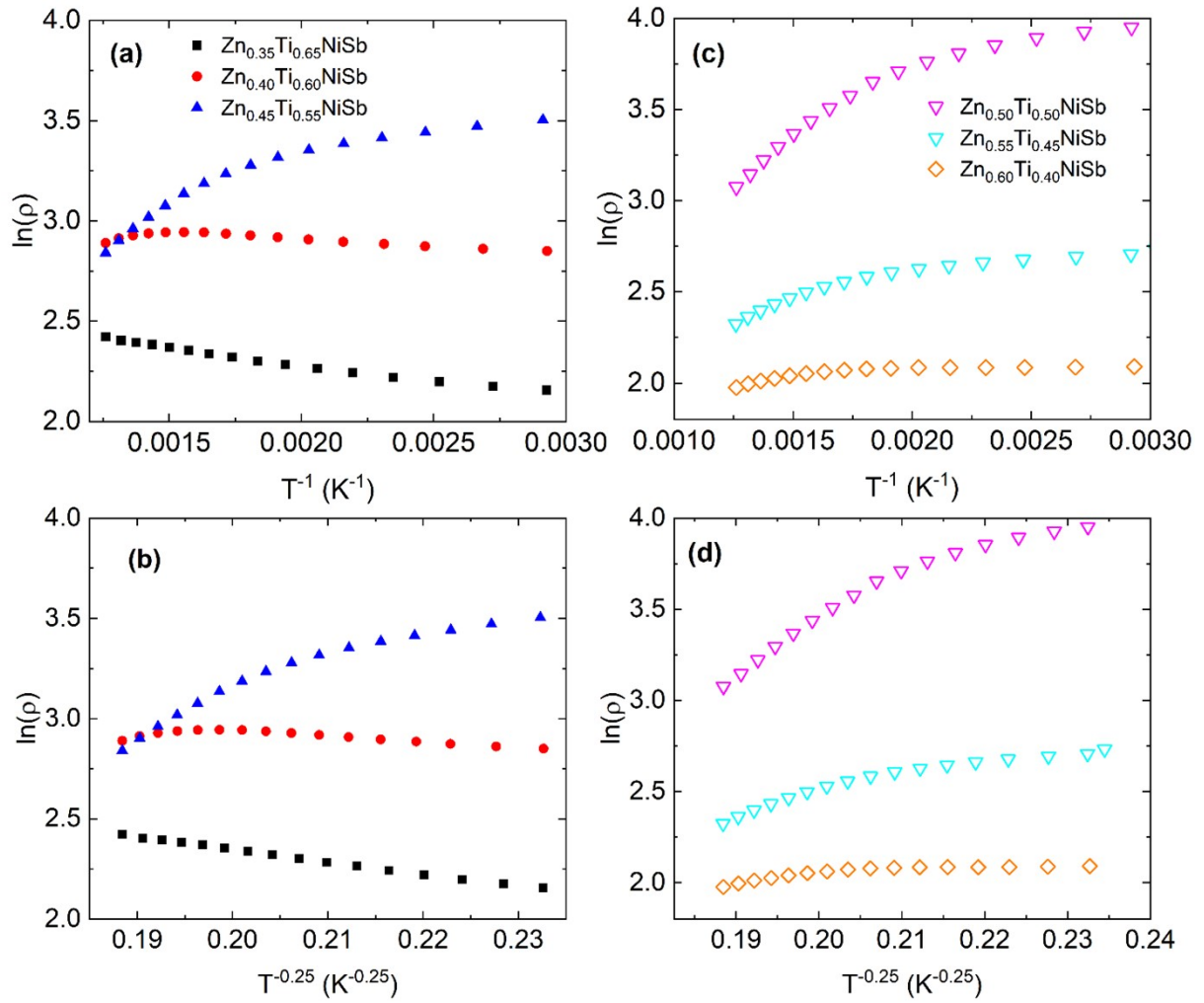


**Figure S3:** Temperature dependence of  $\ln[\rho(T)]$  plotted against  $T^{-1}$  and  $T^{-0.25}$  to check for pure thermally activated semiconducting and variable range hopping transport in **(a-b)** n-type and **(c-d)** p-type  $\text{Zn}_{1-x}\text{Ti}_x\text{NiSb}$ .

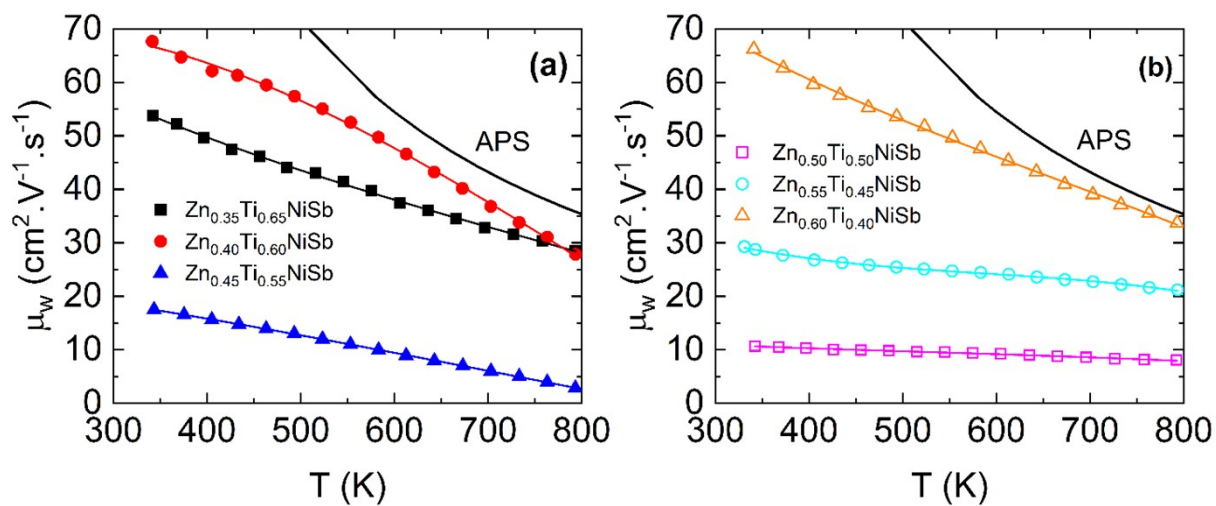


**Figure S4:** Temperature dependence of the weighted mobility ( $\mu_w$ ) calculated from  $S(T)$  and  $\rho(T)$  for (a) n-type and (b) p-type  $\text{Zn}_{1-x}\text{Ti}_x\text{NiSb}$ .<sup>2</sup>

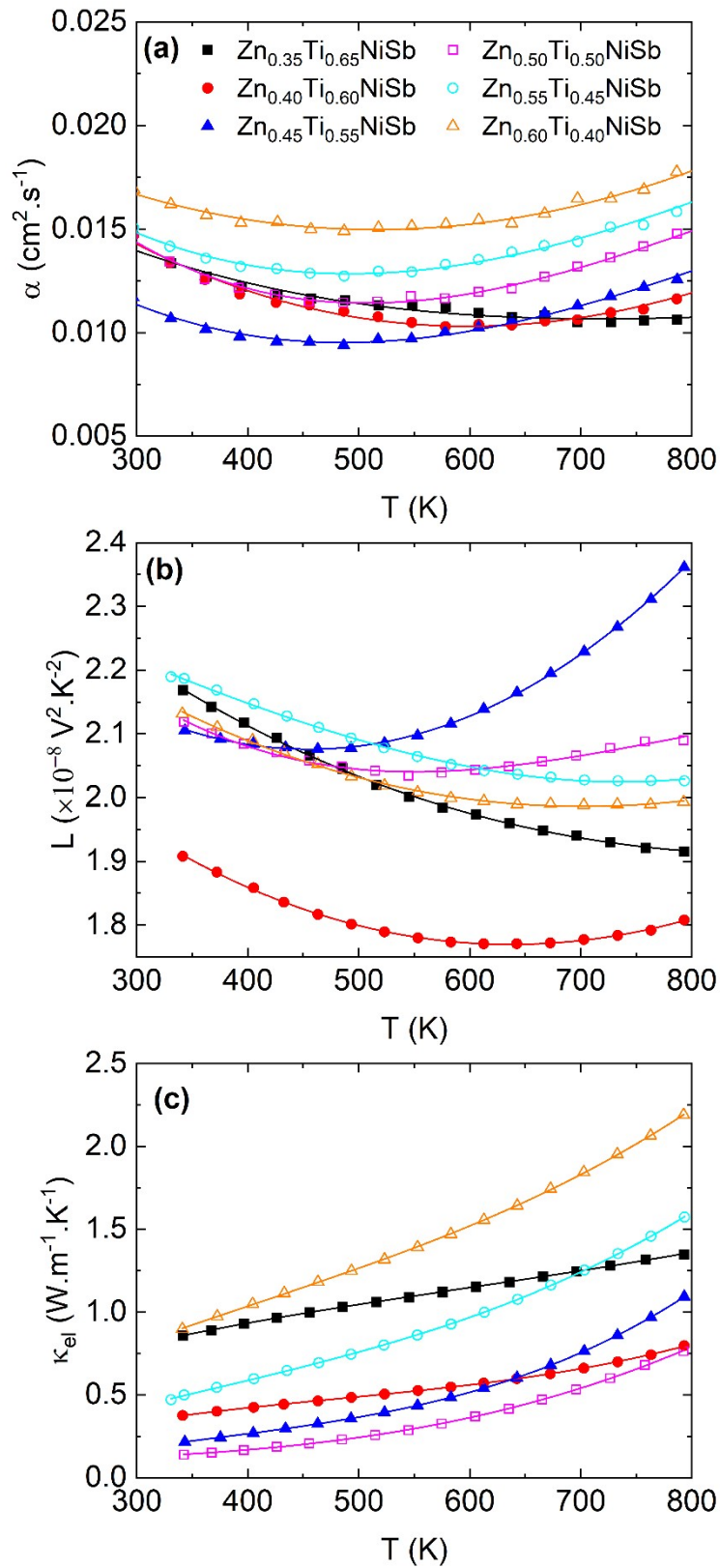


**Figure S5:** Temperature dependence of the (a) thermal diffusivity, (b) calculated Lorenz number,<sup>3</sup> and (c) electronic thermal conductivity ( $\kappa_{el} = LT/\rho$ ) for the Zn<sub>1-x</sub>Ti<sub>x</sub>NiSb samples.



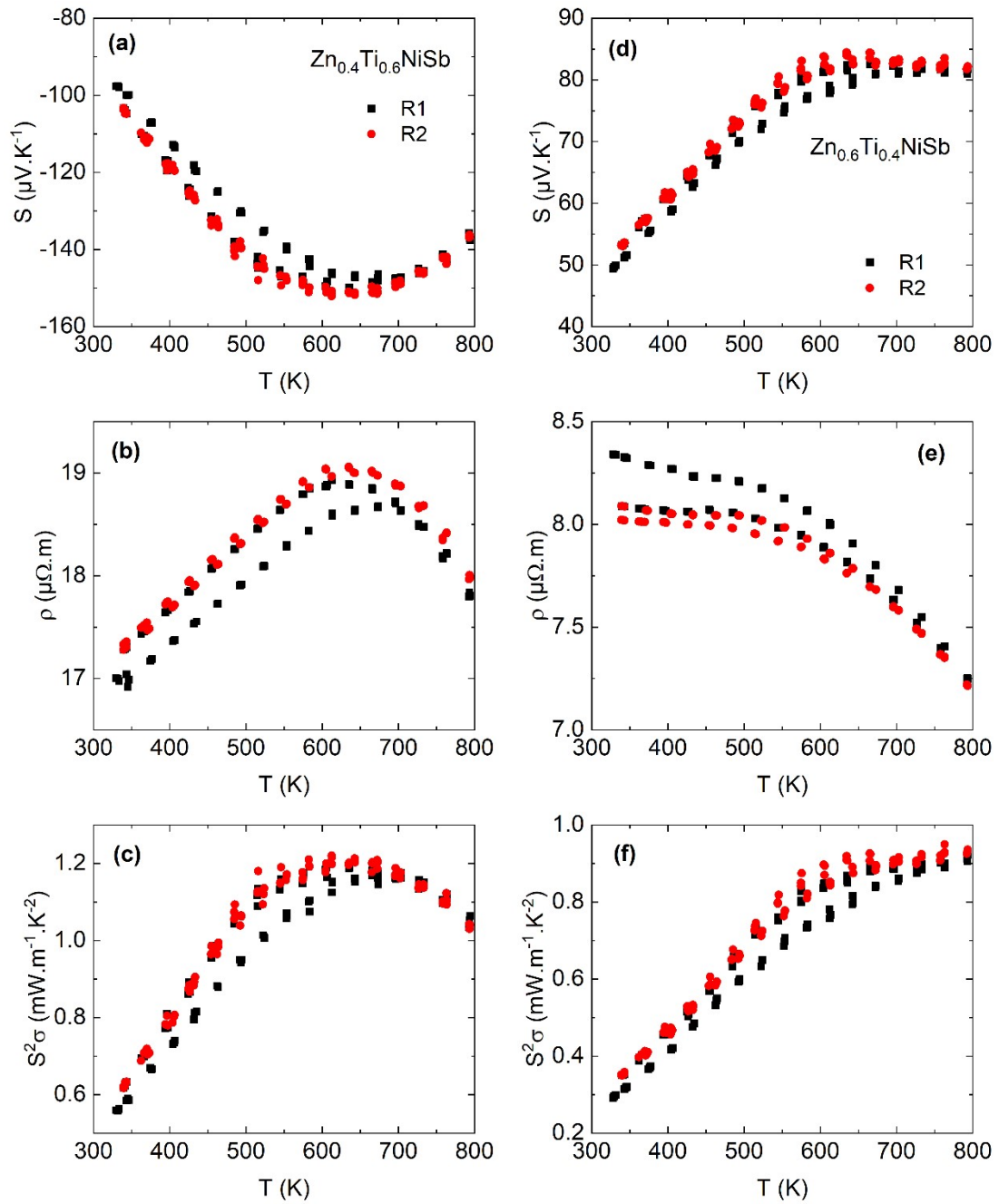


**Figure S6:** Thermal cycling for the best performing n-type  $Zn_{0.4}Ti_{0.6}NiSb$  (a-c) and p-type  $Zn_{0.6}Ti_{0.4}NiSb$  (d-f) samples. The first measurement on heating is slightly offset, but subsequent cooling-heating measurements fall on top of each other.

## References

1. R. J. Quinn, G. B. G. Stenning and J.-W. G. Bos, *Journal of Physics: Energy*, 2022, **4**, 024005.
2. G. J. Snyder, A. H. Snyder, M. Wood, R. Gurunathan, B. H. Snyder and C. Niu, *Advanced Materials*, 2020, **32**, 2001537.
3. H.-S. Kim, Z. M. Gibbs, Y. Tang, H. Wang and G. J. Snyder, *APL Materials*, 2015, **3**, 041506.